INTERNATIONAL JOURNAL FOR NUMERICAL METHODS IN FLUIDS
Int. J. Numer. Meth. Fluids 2001; **36**: 903–923 (DOI: 10.1002/fld.156)

The design of improved smoothing operators for finite volume flow solvers on unstructured meshes

Benjamin de Foy* and William Dawes

Department of Engineering, University of Cambridge, Cambridge, UK

SUMMARY

Spatial operators used in unstructured finite volume flow solvers are analysed for accuracy using Taylor series expansion and Fourier analysis. While approaching second-order accuracy on very regular grids, operators in common use are shown to have errors resulting in accuracy of only first-, zeroth- or even negative-order on three-dimensional tetrahedral meshes. A technique using least-squares optimization is developed to design improved operators on arbitrary meshes. This is applied to the fourth-order edge sum smoothing operator. The improved numerical dissipation leads to a much more accurate prediction of the Strouhal number for two-dimensional flow around a cylinder and a reduction of a factor of three in the loss coefficient for inviscid flow over a three-dimensional hump. Copyright © 2001 John Wiley & Sons, Ltd.

KEY WORDS: accuracy; edge weights; least squares; smoothing operators; tetrahedron; unstructured mesh

1. INTRODUCTION

Unstructured mesh flow solvers using the finite volume methodology are widely applied due to their versatility for problems with complicated geometries; see, for example, Mavriplis [1], Dawes [2], Watterson [3] and de Foy and Dawes [4]. In spite of their frequent use, the accuracy of spatial operators such as the gradient or Laplacian operators used in finite volume solvers has not been fully analysed. It is often assumed that the order of accuracy is the same on a regular unstructured grid as for the corresponding operator on structured meshes, and that this accuracy does not degrade significantly with increasing mesh irregularity. This paper extends current mesh analysis techniques to unstructured meshes so as to verify the above assumptions in the context of the flow solver of de Foy and Dawes [submitted]. A method for determining improved operators is then devised leading to examples of much more accurate flow solutions.

* Correspondence to: Atmospheric Studies Group, Earth Tech Incorporated, 196 Baker Avenue, Concord, MA 01742-2167, U.S.A.

Received 5 November 1998
Revised 25 September 2000

Mesh accuracy analysis for tetrahedral meshes has focussed on geometric quality measures for individual cells. Parthasarathy [4] reviews several of these methods and assesses their ability to detect degenerate cells. They are based on simple ratios of edge lengths, face areas, cell volumes and radii of the circumsphere and inscribed sphere, making them computationally inexpensive to evaluate. These measures can be very effective for both assessing and optimizing meshes.

Accuracy analysis of the actual operator used is relatively less developed. It has, however, attracted considerable attention for finite element methods, with extensive evaluation of interpolation errors for different approximation functions. This provides an estimate of the error involved in the use of an operator given an actual flow solution. Ilinca *et al.* [5] make use of this analysis in two dimensions to redistribute the nodes in a mesh in order to improve mesh resolution without increasing the size of the mesh. Barth and Fredrickson [6] define flow variables as averages over different control volumes around cell vertices and develop higher-order approximations of the flux terms in order to improve accuracy. Later development by Barth [7] makes use of added variable storage at edge centres to support a more accurate reconstruction of the convective flux terms. Comparative analysis by Aftosmis *et al.* [8] of reconstruction techniques on quadrilateral and triangular meshes shows that they have equivalent accuracies despite the extra computational cost of the triangular meshes. The latter, however, perform better when very distorted meshes are used.

For finite volume methods, there have been few attempts at quantifying errors. Roe [9] analyses the accuracy of the gradient operator for triangular meshes in two dimensions and finds it to be second-order accurate for a perfectly regular mesh but usually only first-order accurate on normal meshes. For a mesh where the smoothing operator is at least second-order accurate, Giles [10] shows that global second-order accuracy can be preserved in spite of locally first-order accurate operators, as the truncation errors associated with the flux sums through a face cancel each other out from node to node. Baker [11] analyses the effect on the flow solution of a non-centrally symmetric column of triangular cells based on a rectangular grid of points in two dimensions. The errors of the spatial operators are calculated in a manner similar to Roe and these are then combined with the errors due to the time discretization of the solver. The error introduced is shown analytically to disappear within a few cells for the model convection equation and also for an incompressible boundary layer.

More accurate operators are currently obtained either by higher-order reconstruction for finite volume solvers or by using higher-order elements in finite element solvers. Finite difference schemes are used on Cartesian grids in the field of computational aeroacoustics. For these, high-order accuracy is required in order to propagate accurately as many wave components as possible. This is typically done by using either larger stencils or compact schemes, with up to tenth-order accurate operators. Optimizing for the Fourier behaviour of the operators has been found to be preferable to maximizing the order of accuracy of a solver. This has been implemented by Lele [12] and by Tam and Webb [13]. By reducing the order of accuracy of the operator without reducing the support stencil, extra degrees of freedom are obtained, which are then used for improving the Fourier behaviour of the solvers. Lele does this by specifying the behaviour at certain fixed wave numbers, relying

on a judicious choice of these to guarantee proper behaviour in the range between them. Tam and Webb integrate the error in the effective velocity analytically and minimize it over a predetermined range of wave numbers. Both of these methods deal with centred operators so that there is no artificial dissipation errors to be considered. Two-dimensional results are presented by using the one-dimensional operators in the different Cartesian directions. Lockard *et al.* [14] make use of the method of Tam and Webb to obtain improved operators for an essentially non-oscillatory (ENO) scheme, where the stencil and hence the operator depend on the local flow solution. A later development is included to obtain non-centred schemes, thus removing the need for artificial dissipation or filtering. This requires a weighting function to balance the dispersion errors with the dissipation errors. Kim and Lee [15] extend the analytical method of Tam and Webb to the compact schemes considered by Lele. Further comparison of the two different approaches is presented in Tang and Baeder [16], who develop a method to obtain compact schemes with improved higher frequency solutions.

The smoothing operator is a crucial element of any explicit centred flow solver. Mavriplis [1] adapted the blended second- and fourth-order smoothing of Jameson to unstructured meshes. The second-order term is obtained from an edge sum approximation to the Laplacian. This procedure is then repeated to obtain fourth-order smoothing. Lindquist and Giles [17] compare the order of accuracy of both quadrilateral mesh and triangular mesh flow solvers using the smoothing operator of Mavriplis and a higher-order accurate smoothing operator based on the repeated action of a true Laplacian operator. The higher-order accurate smoothing is found to preserve second-order accuracy, whereas the edge sum smoothing decreases the order of accuracy to 1.5. This, however, comes at the cost of reduced stability for highly stretched meshes. Holmes and Connell [18] seek to improve the edge sum smoothing operator by looking for an approximation to the edge sum procedure that would preserve linear transparency. This is achieved by using Lagrangian multipliers to find edge weights that represent the smallest modification to an edge sum multiplication. In order to preserve sufficient smoothing properties on distorted or stretched meshes, the edge weights are truncated to between 0 and 2, thereby reducing some of the improvements in accuracy. Nevertheless, the method is found to be more robust than the true Laplacian smoothing of Lindquist and Giles [17]. This highlights the trade-off between robustness and accuracy that is often present in the design of smoothing operators, with actors often playing a 'zero sum game'.

These analyses do not, however, extend to the sort of irregularity that is usually present in unstructured meshes. This paper will describe a unified method of formulating operators on any type of mesh using edge sums and then extend Taylor series analysis and Fourier analysis to this framework. The methods will be used to analyse the accuracy of the convection, diffusion and smoothing operators on different types of mesh points. These results do not consider the errors due to the temporal discretization, although they could be used towards a global estimate of accuracy by including them in the analysis of Baker [11].

Having expressed spatial operators as edge sums, a method is presented for designing operators with specific properties on arbitrary meshes. This is applied to the fourth-order smoothing operator of a finite volume flow solver leading to improved accuracy of the solutions.

2. SPATIAL OPERATORS ON UNSTRUCTURED MESHES

The present work is developed within the context of the unstructured, unsteady, incompressible flow solver of de Foy and Dawes [submitted]. This solves the incompressible Navier–Stokes equations with the pressure-correction method of Hirt and Cook [19]. An explicit prediction step (1) is followed by a correction step (2) and (3) based on the pressure Poisson equation (4) and the corresponding velocity correction (5).

$$\mathbf{u}^* = \mathbf{u}^n - \Delta t(\nabla \cdot (\mathbf{u} \otimes \mathbf{u})^n + \nabla p^{n-1} - \nu \nabla^2 \mathbf{u}^n) \tag{1}$$

$$p^n = p^{n-1} + p' \tag{2}$$

$$\mathbf{u}^{n+1} = \mathbf{u}^* + \mathbf{u}' \tag{3}$$

$$\nabla \cdot \nabla p' = \frac{\nabla \cdot \mathbf{u}^*}{\Delta t} \tag{4}$$

$$\mathbf{u}' = -\Delta t \nabla p' \tag{5}$$

where n is the current time level, the prime $'$ is the correction level and ν is the dynamic viscosity.

Cell-vertex storage is used. The variables are nodal values assumed to be piecewise linear within the cells. The gradient operator used to calculate convection fluxes for a variable ϕ defined at all nodes is implemented as a Green–Gauss integration for the control volume comprising all the tetrahedra around a node as shown by Equation (6). V is the volume of all cells around a node and S is the surface area of the same

$$\int_V \nabla \phi \, \mathrm{d}V = \int_S \phi \, \mathrm{d}\mathbf{S} \tag{6}$$

The Laplacian operator, used for the viscous forces, is obtained in two steps. First derivatives are obtained by applying Green–Gauss integration for individual tetrahedra. These values are then used in a Green–Gauss integration over the median dual (M, surface area S_M) around a node as described by Equation (7)

$$\int_M \nabla^2 \phi \, \mathrm{d}V = \int_{S_M} \nabla \phi \cdot \mathrm{d}\mathbf{S} \tag{7}$$

Because the discretization of the flow solver is centred in space and forward in time, explicit artificial dissipation is added at each time step. The method of Mavriplis [1] is used, applying a blend of second- and fourth-order smoothing. A second difference is constructed as an approximation to the Laplacian using the edge sum procedure described by Equation (8). For a variable ϕ defined at all nodes, the second difference is the sum of the difference over all edges connecting a central node k to its first neighbours n

$$d^2\phi_k = \sum_n (\phi_k - \phi_n) \tag{8}$$

The process is then repeated on the second differences in order to obtain an approximation to a fourth difference

$$d^4\phi_k = \sum_n (d^2\phi_k - d^2\phi_n) \tag{9}$$

On a Cartesian grid, the above equations yield a second and fourth difference operator. For unstructured meshes, however, they are a coarse approximation of these operators and are retained mainly because of the ease of their implementation and their effectiveness at eliminating flow instabilities. Artificial dissipation is added to the velocity field on the right-hand side of the prediction step (1) ensuring that continuity is preserved, and to the pressure field when it is updated with the pressure correction (2).

3. ACCURACY ANALYSIS

3.1. Edge weights

In order to facilitate the accuracy analysis and enable further developments of different types of operators, we seek to represent these as edge sums as described by Equation (10). An operator A acting on a nodal variable field ϕ returning a value at node k can be represented as a sum of the value at each neighbour n of node k multiplied by a coefficient C_n. C_k is the coefficient of the impact of the value of ϕ_k on $(A\phi)_k$ and equals $-\Sigma_n C_n$

$$(A\phi)_k = C_k\phi_k + \sum_n C_n\phi_n \tag{10}$$

Application of any type of operator, whether it be the simple edge sum smoothing operator described above (in which case $C_n = 1$ for all n) or the finite volume gradient or Laplacian operators, then reduces to a matrix multiplication with different sets of coefficients and different sets of edges. For the fourth-order smoothing operator, the set of neighbours will include all of the second neighbours of a node, not just the set of neighbours sharing a cell edge with the central node.

This is equivalent to rephrasing any type of scheme into a finite difference formulation. Different operators can then be accommodated in any number of dimensions by appropriately constructing the list of edges and determining the value of the edge weights corresponding to the desired operator.

3.2. Taylor analysis

Having obtained the edge sum equivalent of an operator, the Taylor series equivalent can be determined by substituting a Taylor expansion of the variable field around node k. This is

shown to second-order in Equation (11) for a variable ϕ at neighbouring nodes n, where $\Delta\mathbf{r}_{kn}$ is the vector length from k to n and $\mathscr{H}_k$ is the Hessian matrix

$$\phi_n = \phi_k + \Delta\mathbf{r}_{kn}^T \nabla\phi_k + \frac{1}{2}\Delta\mathbf{r}_{kn}^T \mathscr{H}_k \Delta\mathbf{r}_{kn} \tag{11}$$

Substituting Equation (11) into Equation (10) leads to an equation for each term in the Taylor series expansion in terms of the edge weights as shown in Equation (12). The indices i, j, k correspond to the derivatives in the x-, y-, z-directions and the terms Δx_n, Δy_n, Δz_n are the Cartesian components of the edge length $\Delta\mathbf{r}_{kn}$

$$a_{i,j,k} = \sum_n C_n \Delta x_n^i \Delta y_n^i \Delta z_n^k, \quad i,\ j,\ k = 0,\ 1,\ 2 \tag{12}$$

By evaluating the terms of the Taylor series expansion, the order of accuracy of any operator can be easily determined. The actual behaviour of the operator is, however, difficult to interpret from the magnitude of the terms in the series.

3.3. Fourier analysis

The Fourier behaviour of the operator can be obtained by substituting a Fourier expansion for variable ϕ around node k in Equation (10). This has been used by Lele [12] and by Tam and Webb [13] in the field of computational aeroacoustics to develop operators with improved wave transport properties.

In one dimension a flow solution can be written as a Fourier series (13), with wave numbers k_l given by Equation (14), where Δs corresponds to the mesh spacing and N is the number of terms in the series for a regular one-dimensional stencil with $2N+1$ nodes

$$\phi(s) = \sum_{l=0}^{N} \hat{\phi}_l \, \mathrm{e}^{ik_l s} \tag{13}$$

$$0 < k_l < \frac{\pi}{\Delta s} \tag{14}$$

Substituting this into the edge weight formulation of an operator leads to the following equation:

$$(A\phi)_k = C_k \sum_{l=0}^{N} \hat{\phi}_l + \sum_n C_n \sum_{l=0}^{N} \hat{\phi}_l \, \mathrm{e}^{ik_l s_n} \tag{15}$$

The summation terms over the edges can be performed numerically, leaving an expression for the behaviour of the operator in terms of the wave number

$$(A\phi)_k = \sum_{l=0}^{N} k^* \hat{\phi}_l \, \mathrm{e}^{ik_l s} \tag{16}$$

k^* is referred to as the modified wave number and is a function of the wave number, describing the effect of the operator on each term in the Fourier series. It contains a real part describing the diffusion of the Fourier term and an imaginary part describing the convection.

In order to analyse the behaviour of the operator, it is necessary to compare the modified wave number with the wave number corresponding to the ideal operator. Taking the ideal gradient operator as the first derivative in s, the desired wave number can be shown to be

$$k^{\mathrm{conv}} = \mathrm{i}k_l \tag{17}$$

Solving the semi-discretized convection equation with the finite difference gradient operator and comparing this with the solution of the convection–diffusion equation yields the following expression for an effective wave speed and effective viscosity of the convection operator:

$$u^* = u \frac{k_i^*}{k_l} \tag{18}$$

$$\mu^* = u \frac{k_r^*}{k_l^2} \tag{19}$$

This shows that the ratio of the imaginary part of the modified wave number to the wave number describes the accuracy with which that particular wave component will be convected. This ratio tends to zero at the Nyquist frequency. The real part of the modified wave number characterizes the dissipation error of the operator. In order to obtain a meaningful expression from the effective viscosity, it is expressed as a modified Reynolds number. The dissipation error can be compared with the magnitude of the convection operator such that the error can be quantified as the inverse of the effective Reynolds number as follows:

$$\frac{\mu^* \dfrac{\partial^2 u}{\partial s^2}}{u \dfrac{\partial u}{\partial s}} \approx \frac{\mu^* \dfrac{u}{\Delta s^2}}{u \dfrac{u}{\Delta s}} = \frac{\mu^*}{u \Delta s} = \frac{1}{Re^*} \tag{20}$$

The lower the effective Reynolds number, the higher the error. An effective Reynolds number of 2 corresponds to the diffusion associated with the first-order upwind scheme.

For the diffusion operator a second derivative is desired, leading to the following ideal wave number:

$$k^{\mathrm{diff}} = -k_l^2 \tag{21}$$

An analysis similar to that of the gradient operator leads to an effective viscosity and wave speed as follows, where the effective viscosity is now the desired term and the effective velocity the error term

$$\mu^* = -\mu \frac{k_r'}{k_l^2} \tag{22}$$

$$u^* = -\mu \frac{k_i'}{k_l} \tag{23}$$

The effective viscosity should be equal to the actual viscosity and the effective wave speed should be zero. To quantify the convective error terms, an effective Reynolds number is obtained based on the effective wave speed and the actual viscous term

$$\frac{u^* \dfrac{\partial u}{\partial s}}{\mu \dfrac{\partial^2 u}{\partial s^2}} \approx \frac{u^* \dfrac{u}{\Delta s}}{\mu \dfrac{u}{\Delta s^2}} = \frac{u^* \Delta s}{\mu} = \frac{k_i' \Delta s}{k_l} = Re^* \tag{24}$$

In order to quantify the errors, the convective error can be compared with the true convective term leading to a relation linking the effective Reynolds number to the cell Reynolds number

$$\frac{u^*}{u} = -\frac{\mu k_i'}{u k_l} = -\frac{\mu}{u \Delta s} \frac{k_i' \Delta s}{k_l} = -\frac{1}{Re_c} Re^* \tag{25}$$

The cell Reynolds number in actual flow solutions will vary from infinity for inviscid flow to a value around unity in viscous layers. If a value of 2 is taken as representative of points in areas of viscous flow, the effective Reynolds number can be interpreted as being twice the ratio of the convective error term to the true convection term.

A three-dimensional Fourier expansion with different wave numbers in each of the Cartesian directions could be used to analyse the behaviour of general operators. This, however, eliminates the ease of interpretation afforded by the above scheme. A single wave in an arbitrary direction can be represented as the sum of three waves in each Cartesian direction. A three-dimensional Fourier analysis can therefore be performed by modifying the direction of s, which is the equivalent of decomposing the analysis for each Cartesian direction and combining the results for any possible direction. Zingg and Lomax [20] do this in two dimensions, plotting the results in polar co-ordinates for each wave direction in the plane. For three dimensions, polar plots are made for two-dimensional slices in space. Cuts in the x–y plane and the x–z plane are used to partially represent the three-dimensional behaviour. For the gradient operator, the ratio k_i^*/k_l is plotted in the radial direction to represent the wave speed, and e^{1/Re^*} for the effective viscosity. For the dissipation operator, the ratio k_r^*/k_l^2 describes the viscous behaviour and e^{Re^*} is plotted for the dispersion errors. These variables have been chosen so as to be always positive, with desired values of 1, so that inaccuracies can be seen as departures from the unit circle.

The maximum wave number is based on the minimum edge length around a node, although this may not be representative in cases were the mesh is very irregular or anisotropic. In these instances, a case by case approach needs to be adopted when analysing the behaviour.

4. ANALYSIS RESULTS

4.1. Gradient operator

First, a regular mesh point will be considered. An approximation to this is obtained in three dimensions by extruding a regular two-dimensional mesh. The Fourier behaviour for the x–y and x–z plane is shown in Figure 1 along with a cut of the mesh in the corresponding plane. Trace 1 corresponds to the lowest wave number, close to a constant component, and trace 7 corresponds to the Nyquist frequency.

The decreasing radii of the plots of effective wave speed with increasing wave number show the reduction in the response of the operator, reaching zero for the Nyquist frequency. The response is very isotropic, with the six points around the node in that plane yielding considerable improvements over a regular Cartesian grid. Anisotropies develop rapidly with

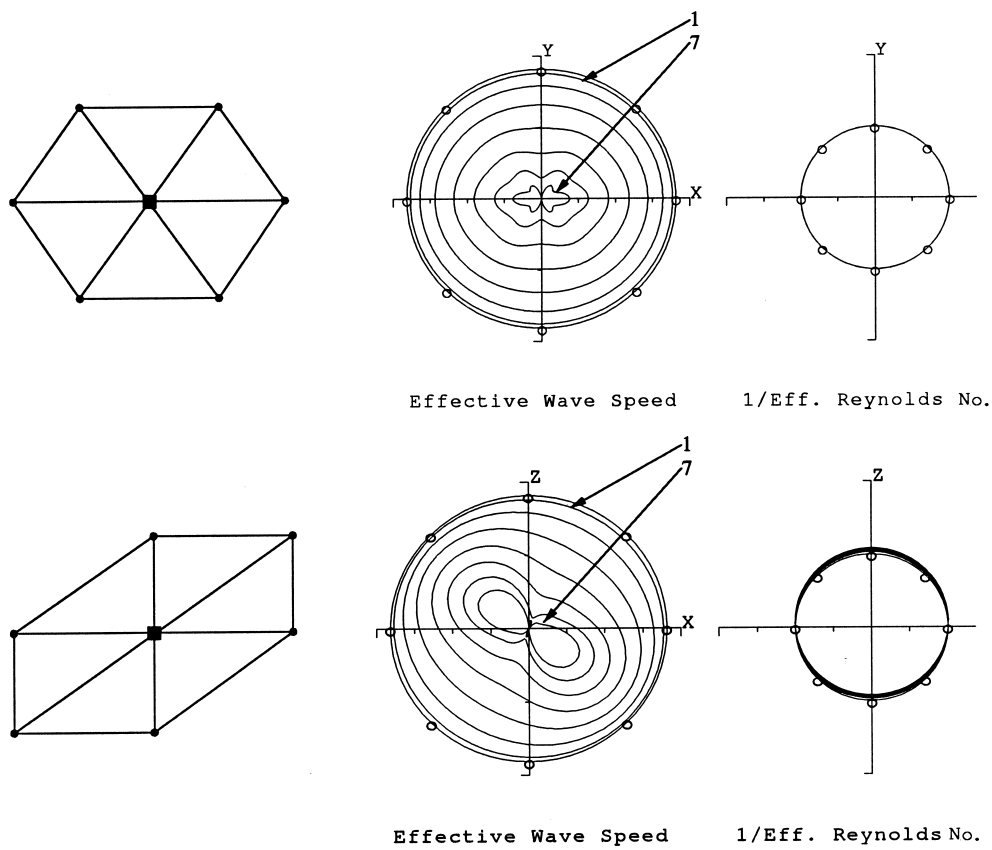

Figure 1. Stencil and Fourier plot for the convection operator on a regular mesh in the x–y and x–z planes.

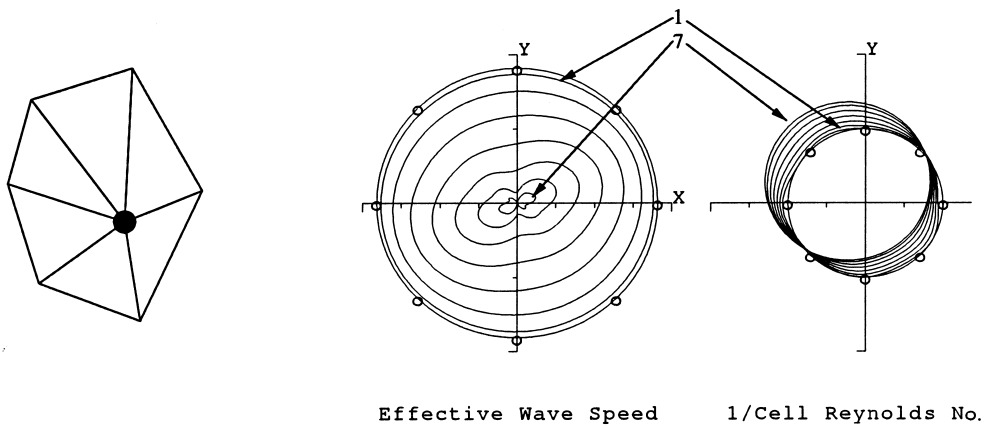

Figure 2. Stencil and Fourier plot for the convection operator on a distorted mesh.

decreasing regularity, however, as shown by the plot for the x–z plane. While there is very little dissipation error in the x–y plane, the error increases in the x–z plane to a value corresponding to a minimum effective Reynolds number of 13. Figure 2 shows the results in the x–y plane for a mesh point with 20 per cent randomization used to represent a realistic unstructured mesh. The convective behaviour remains remarkably isotropic, but significant levels of dissipation are introduced. The effective Reynolds numbers are as low as 3.5, suggesting that the dissipation errors are half that of a first-order upwind operator.

4.2. Laplacian operator

The repeated action of a first-order accurate operator can be shown to be zeroth-order accurate, meaning that the Laplacian operator will contain errors in the coefficients of the second derivatives themselves. For the distorted mesh point considered above, Taylor series analysis shows the coefficients of the second derivative terms to be 1.11, 0.98 and 1.05 for the x-, y- and z-directions and the coefficients of the cross-derivative terms (xy, xz and yz) to be 0.24, 0.52 and 0.59. This is confirmed by the Fourier analysis showing errors in the effective velocity of nearly 15 per cent, even at low wave numbers, and dispersion errors that can reach 20 per cent of the true convective term for an assumed cell Reynolds number of 2. Looking at the actual coefficients of the operator themselves, 4/14 are found to be negative. Even for the regular mesh point, positivity is not satisfied, explaining the lack of robustness displayed by this operator when used for smoothing.

4.3. Second-order smoothing

Application of the Taylor series analysis to the second-order smoothing operator (8) shows that the first derivative terms do not vanish on normal unstructured meshes. Dividing the second difference by a length scale squared will lead to errors of order of accuracy of -1.

Furthermore, slight anisotropies in the mesh lead to very different coefficients of the second derivative terms in different directions. In practice, the situation is tempered by the magnitude of the smoothing coefficients and by the Fourier behaviour of the operator.

This is shown in Figure 3 for the distorted mesh point considered above, where the results are scaled to fit in the unit circle. This shows that even though the mesh cannot be considered a stretched mesh, considerable anisotropy arises in the dissipative behaviour. Dispersion errors correspond to 40 per cent of the true convection term for a cell Reynolds number of 2, so that significant corruption of the flow solution is liable to occur.

In all cases considered, however, whether on the boundary or in highly stretched meshes, the dissipation is positive. This is to be expected as the coefficients are all positive by definition, and explains the operator's popularity as a robust smoother.

4.4. Fourth-order smoothing

Taylor analysis of the fourth-order operator (9) on regular meshes shows that even for these there are non-zero terms for all of the derivatives in the Taylor series and that the first and second derivative terms are at least an order of magnitude greater than the desired fourth derivative terms.

Figure 4 shows the Fourier behaviour of the operator for the distorted mesh point D in Figure 5, scaled so as to fit on the unit circle. Ideally, the effective viscosity is zero for low wave numbers and increases thereafter. In this case, there is a clear trend of increasing viscosity with wave number, but it is not zero at the low wave numbers and decreases for the highest wave numbers. This is due to the presence of second derivative terms. Despite the inaccuracy of the operator, however, the smoothing is positive everywhere and relatively isotropic. As for the dispersion errors, these are shown to be very large. To assess their importance, the magnitude of the numerical viscosity coefficient was evaluated for specific nodes in real flow solutions so as to compare the dispersive error with the true convection term. This showed that

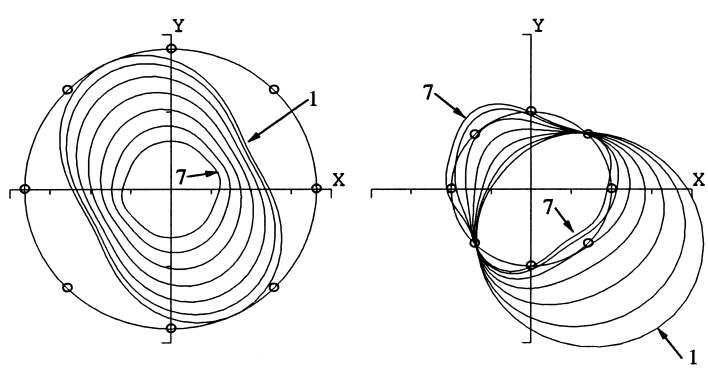

Figure 3. Fourier plot for the edge sum Laplacian operator on a distorted mesh.

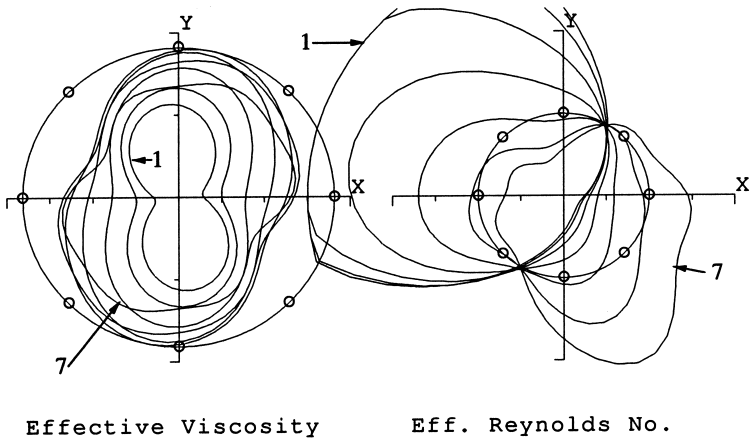

Figure 4. Fourier plot for the fourth-order edge sum smoothing operator on distorted mesh point D.

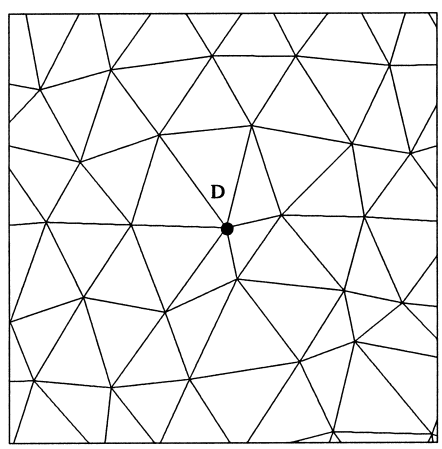

Figure 5. Mesh stencil for irregular point D in the x–y plane.

the values of the effective Reynolds number corresponded to errors of 45 per cent for this particular mesh point. Direct comparison of the convection term with the smoothing term for a converged solution confirmed this result. As the errors are generated by the first derivative terms, they occur for the low wave numbers, which are the ones most likely to be present in the solution.

Figure 6 shows the Fourier behaviour at a point in a viscous layer. The mesh, taken from an airfoil geometry, is an extruded rectangular mesh with an aspect ratio of 15. One would

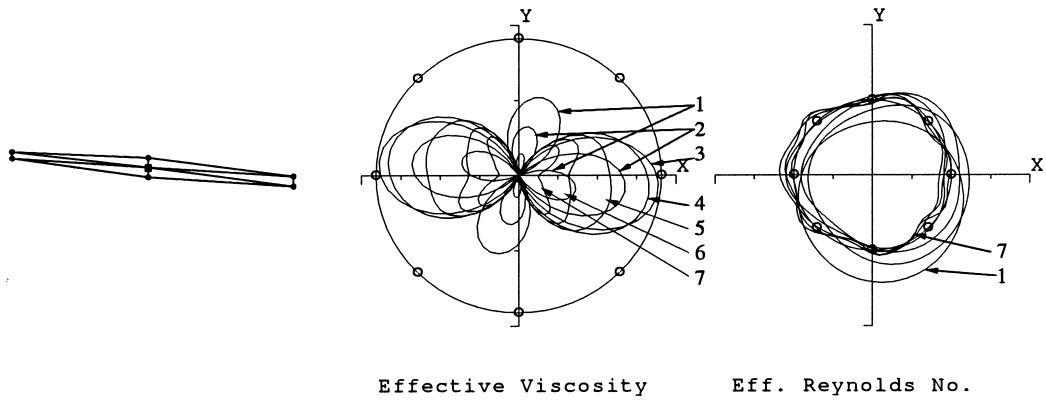

Figure 6. Stencil and Fourier plot for the fourth-order smoothing operator on point i in a viscous layer.

expect, and even desire, anisotropic smoothing for this mesh. In addition to this, however, there is negative smoothing at low wave numbers. This was found on other cases containing stretched meshes and is common for nodes on boundaries or at boundary edges. The dispersion errors in this case are lower, due in part to the greater regularity of the mesh and in part to the fact that the effective Reynolds number is based on the longest edge length meeting at the node.

5. DESIGNING EDGE WEIGHTS

Severe limitations were revealed by the analysis described above for operators routinely used in practice. Having expressed the operators as edge sums, it is possible to treat these as adjustable parameters in an algebraic system with as many degrees of freedom as there are edges. This will be described in the context of the fourth-order edge sum smoothing operator.

The performance of an operator is limited by its support stencil, defined as the set of all the neighbouring nodes connected to a central node by an edge. Finite volume operators are usually limited to their first neighbours as defined by all nodes sharing an actual cell; this set contains of the order of 10–20 nodes. The fourth-order smoothing operator, however, makes use of all of the second neighbours of a node, which can be up to 100 nodes depending on the mesh. Since the term 'edge' no longer refers to the physical edge of a cell, edges can be created linking any two points together, thereby extending the definition of the operator and adding an extra degree of freedom to its behaviour. Given this flexibility, many strategies exist for increasing a support stencil. In two dimensions, the support stencil for the fourth-order smoothing operator was defined as the set of all second neighbours. In three dimensions, however, the first neighbours were included and 'tentacles' were extended in the six Cartesian directions as shown in Figure 7. This leads to many fewer points than the second neighbours but allows the construction of an operator of similar order of accuracy.

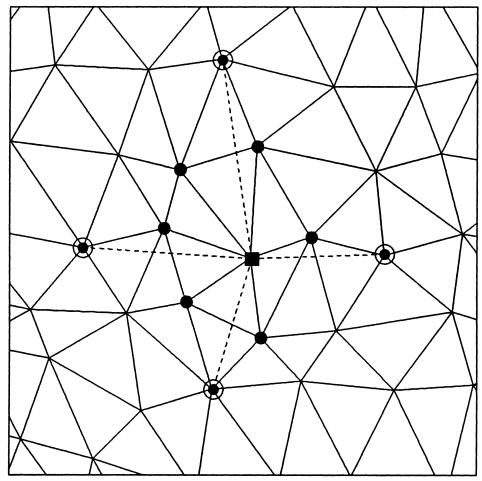

Figure 7. Adding tentacles to the stencil of a node.

Having determined the support stencil, the determination of the coefficients can be cast as an optimization problem. Constraints on the minimum behaviour of the operator are implemented as a system of linear equations and the desired behaviour is translated into a set of functions to be minimized. Using least-squares optimization, the whole system of equations is described by Equation (26) for a vector $\mathbf{x}$ of size n containing the coefficients C_n

$$\text{Minimise } F(\mathbf{x}) \quad \text{subject to } \mathbf{l} \leq \begin{Bmatrix} \mathbf{x} \\ C\mathbf{x} \end{Bmatrix} \leq \mathbf{u} \tag{26}$$

where

$$F(\mathbf{x}) = \frac{1}{2} \|\mathbf{b} - A\mathbf{x}\|^2 \tag{27}$$

$\mathbf{l}$, $\mathbf{u}$ are the lower and upper limits for constraints; C is a $n_c \times n$ constraints matrix; n_c is the number of constraints; $\mathbf{b}$ is the vector of observation; A is an $n_m \times n$ least-squares matix; n_m is the number of minimizations.

This framework allows for three types of controls on the specification of the edge weights: constraints on the magnitude of the coefficients (in $\mathbf{l}$ and $\mathbf{m}$), constraints on the behaviour of the coefficients (in C, $\mathbf{l}$ and $\mathbf{u}$) and optimization of the behaviour of the coefficients (in A and $\mathbf{b}$).

Constraints on the magnitude of the coefficients are used to prevent degenerate cases as well as to ensure certain numerical behaviour. In order to obtain a robust second-order smoother,

the coefficients could be constrained to being positive. Since the fourth-order smoother contains negative coefficients, even on a Cartesian mesh, no limits were imposed for the optimized operator.

Constraints on the behaviour of the operator were applied to its Taylor series expansion. This is the usual method of obtaining finite difference operators, specifying as high an order of accuracy as the support stencil will allow. While this is satisfactory on Cartesian grids, on irregular unstructured grids constraints on the lower derivatives can lead to very high truncation errors of the higher derivative terms for certain cases. In order to ensure linear transparency for the smoothing operator, all the terms in the Taylor series up to and including the third derivative were set to zero. No constraints were imposed on the fourth derivative terms.

The determination of the smoothing behaviour of the operator relies entirely on the optimization of its Fourier behaviour. The optimum operator was chosen to be the exact fourth-order smoothing operator on a Cartesian grid, described by coefficients $(1, -4, 6, -4, 1)$. This is consistent with the Taylor series constraints imposed on the operator as well as with the support stencil constructed for each node. The modified wave number relations for this operator are given by

$$k_i = 0$$

$$k_r = \Delta s^4 k_l^4 - 0.1667\Delta s^6 k_l^6 + 0.0125\Delta s^8 k_l^8 - 5.622 \times 10^{-4}\Delta s^{10} k_l^{10} + 1.709 \times 10^{-5}\Delta s^{12} k_l^{12} - 3.758 \times 10^{-7}\Delta s^{14} k_l^{14} + \text{HOT} \tag{28}$$

Departures from these relations were minimized over a set of discrete wave numbers and directions representing three-dimensional space. Figure 8 depicts the wave directions chosen where θ represents the angle in the x–y plane and ϕ is the elevation from this plane. These directions were reflected in the x–y plane, thereby spanning one hemisphere, which is all that is needed due to the presence of a plane of symmetry in the Fourier analysis. Three wave numbers were chosen between 0.4 and 0.9 of the Nyquist frequency. For the uniform meshes,

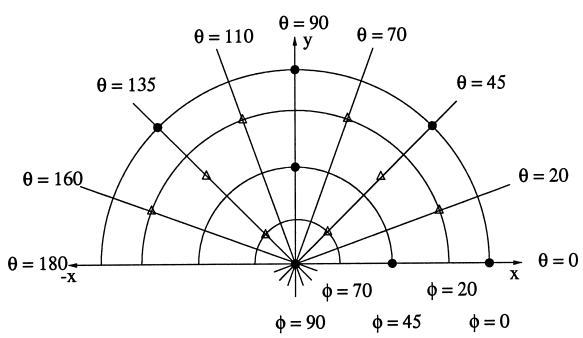

Figure 8. Wave directions in three-dimensional space, angles in degrees.

the Nyquist frequency was defined based on the average edge length, whereas for irregular or stretched meshes, the definition was based on the root-mean-square (r.m.s.) of the mesh spacing projected in each particular wave direction.

6. BOUNDARIES

Special treatment is required at and next to boundaries as the stencil there is not able to support fourth-order smoothing. For simplicity, second-order smoothing operators were obtained on boundaries and error terms were allowed in the first derivative in the wall normal direction. These specifications are the same as the implicit ones for the second-order edge sum smoothing operator. For nodes one cell away from boundaries, fourth-order smoothing was enforced in directions tangent to the wall in the same manner as for nodes inside the flow domain. Normal to the wall, the desired operator was a combination of second- and fourth-order smoothing with zero error in the first gradient terms following the operators described by Pulliam [21].

7. RESULTS

The Fourier behaviour of the new smoothing operator is presented for an equilateral mesh in Figure 9. As before, trace 1 corresponds to the lowest wave number and trace 7 to the Nyquist frequency. This shows that the operator is very isotropic and has a very low response at the low wave numbers. Figure 10 shows the Fourier behaviour of the optimized operator for the distorted mesh point D shown in Figure 5. The Fourier behaviour of the edge sum operator

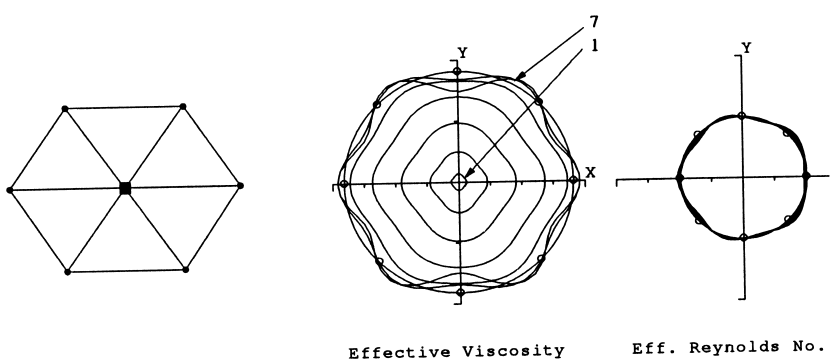

Figure 9. Fourier plot for the two-dimensional optimized fourth-order smoothing operator on a regular mesh point.

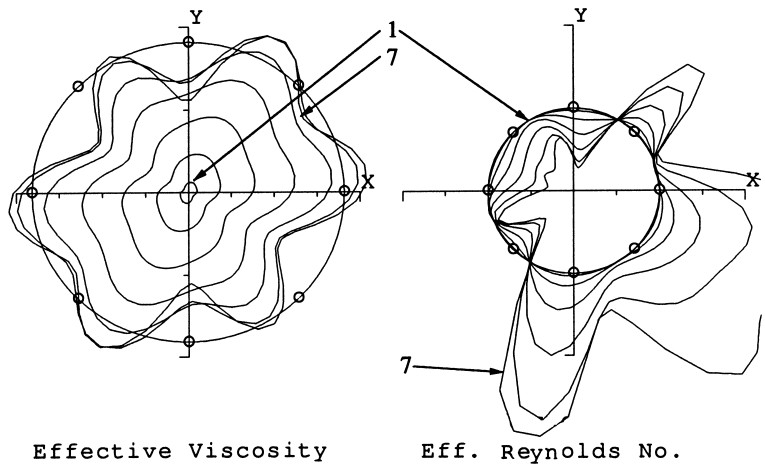

Figure 10. Fourier plot for the two-dimensional optimized fourth-order smoothing operator on irregular mesh point D.

was shown in Figure 4. From this it can be seen that the new operator contains no smoothing at the low wave numbers and more isotropic smoothing at higher wave numbers. The dispersion error is totally eliminated for the low wave numbers and increases steadily to substantial values at the Nyquist frequency. The higher frequency waves are, however, suppressed by the smoothing such that the dispersion errors will not affect the global accuracy of the flow solution.

The smoothing was applied to the calculation of unsteady vortex shedding behind a cylinder. Trials with the edge sum operator had led to an underestimation of the Strouhal number for flows in the Reynolds number range of 100–250. This was thought to be due to the presence of smoothing at the low wave numbers leading to a lower apparent Reynolds number as well as to the dispersion errors. Table I provides a comparison of the drag and lift coefficients with the results of Belov *et al.* [22]. These computational results were obtained using a

Table I. Strouhal number, drag coefficient and lift coefficient at $Re = 200$ with edge sum and Fourier optimized smoothing along with results from Belov *et al.* [22].

Calculation	Strouhal number	C_D	C_L
Edge sum	0.177	0.88 ± 0.029	± 0.47
Fourier optimized	0.192	0.95 ± 0.038	± 0.55
Belov *et al.* [22]	0.193	1.19 ± 0.042	± 0.64

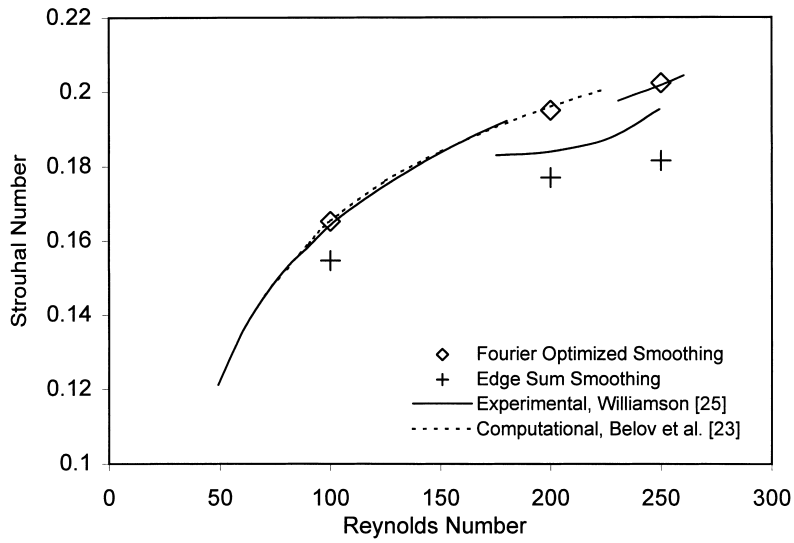

Figure 11. Strouhal number versus Reynolds number for vortex shedding behind a cylinder (adapted from Belov *et al.* [24]).

two-dimensional solver with an 'O' mesh of (256×256) nodes and showed very good agreement with published experimental and numerical values. The improvement using the optimized operators is clearly shown. The remaining discrepancy is thought to be due to numerical approximations involved in the evaluation of viscous stresses at the boundary during the calculation of the lift and drag coefficients.

Figure 11 shows the improvement in the calculation of the Strouhal number at three different Reynolds numbers of the Fourier optimized smoothing compared with the edge sum smoothing and with published experimental and computational results.

Inviscid flow over a hump served as a test case with truly three-dimensional smoothing operators even though the flow is two-dimensional. The mesh was constructed by extruding a two-dimensional mesh to create a domain three cells thick with the middle plane shown in Figure 12. The nodes in the individual planes were randomized by 20 per cent so as to simulate the kind of mesh irregularity that might be found in more realistic problems.

The results in Figure 12 for the mesh with the mid-plane shown in Figure 13 show much improved symmetry in the flow solutions. Table II shows that the global pressure loss coefficient, defined as the non-dimensionalized mass flux integral of the stagnation pressure, is a third of that which is obtained using either the edge sum smoothing operator or the optimized operator of Holmes and Connell [18].

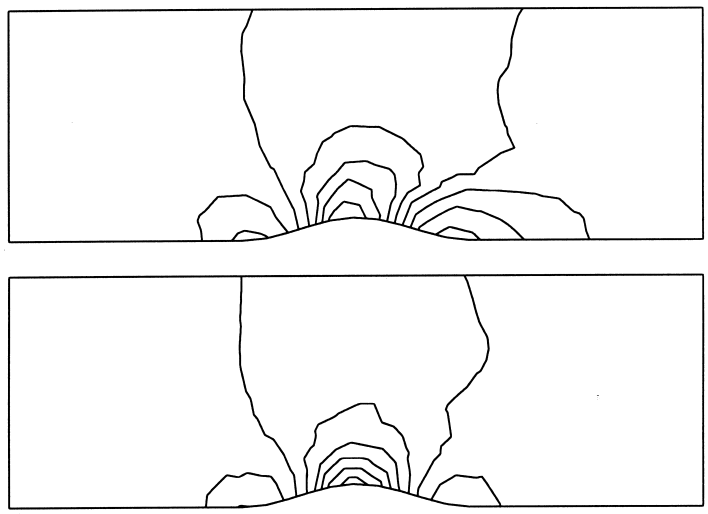

Figure 12. Contours of x-velocity for inviscid hump with fourth-order edge sum (top) and optimized (bottom) smoothing.

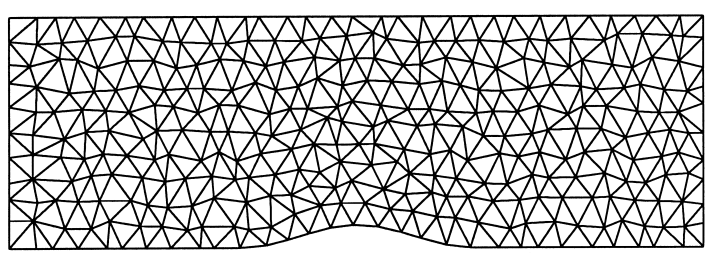

Figure 13. Randomized hump mesh.

Table II. Global pressure loss coefficient for three-dimensional inviscid flow over a hump with three types of fourth-order smoothing operators.

Fourth-order smoothing operator	Global pressure loss coefficient
Edge sum	0.0050
Holmes and Connell [18]	0.0048
Fourier optimized	0.0016

8. CONCLUSION

Making use of a generalized edge weight formulation for operators enabled unified accuracy analyses of any type of operator based on both Taylor series analysis and Fourier analysis. This analysis remains local in nature and was applied solely to the errors introduced by the spatial operators. The local error terms could however be used as inputs to the method of Baker [11] to obtain a global estimate of error that would also take into account the temporal discretization errors.

The finite volume gradient operator based on a control volume comprising all cells meeting at a node was shown to be nearly second-order accurate on a very regular mesh but was much more likely to be of first-order accuracy on a realistic mesh with error terms on a par with an upwind discretization. The direction of waves for which the dissipation error is positive is, however, totally grid-dependent and can be opposite to the local flow direction. This leads to substantial anti-smoothing at some nodes and explains the observation that unstructured flow solvers develop instabilities faster than their structured counterparts and require higher levels of artificial dissipation.

The Laplacian operator was found to be zeroth-order accurate rather than second-order with errors in the second derivative term of up to 50 per cent of the desired value on irregular meshes. In addition, positivity of coefficients is not satisfied on even the most regular grids, leading to lack of robustness when the operator is used for smoothing and convergence problems when it is used to solve the Poisson equation.

The edge sum approximation to the Laplacian is frequently used as a smoothing operator. As such, its accuracy is only of secondary importance compared with the requirement that it yield positive smoothing for all flows. Fourier analysis showed that this was the case for most meshes for the second-order smoothing operator. The fourth-order smoothing operator was a little more sensitive, yielding negative smoothing for very distorted meshes. In terms of accuracy, however, both fared particularly poorly with substantial errors in the first and all subsequent derivatives. This means that the second-order smoothing operator, when scaled by a volume term, had an order of accuracy of -1. After including the coefficients of numerical dissipation, this led to smoothing of zeroth-order accuracy.

A general framework was proposed for determining any type of operator on unstructured meshes based on an edge sum formulation using least-squares optimization. This was applied to the fourth-order smoothing operator. In two dimensions, results for unsteady vortex shedding showed a great improvement in accuracy while in three dimensions the loss coefficient for inviscid flow over a hump was reduced by a factor of three. The scheme can be extended to different operators, such as the gradient and Laplacian operator. This would enable a 'mesh free' flow solver consisting of a collection of points with connecting edges chosen based on the desired accuracy of the flow solution.

ACKNOWLEDGMENTS

The first author is very grateful to St John's College, Cambridge, for support via a Benefactor's Scholarship and for a grant from the EPSRC, UK. The research in this paper was performed at the Whittle Laboratory.

REFERENCES

1. Mavriplis DJ. Accurate multigrid solution of the Euler equations on unstructured and adaptive meshes. *AIAA Journal* 1990; **28**(2): 213–221.
2. Dawes WN. Simulation of three-dimensional viscous flow in turbomachinery geometries using a solution-adaptive unstructured mesh methodology. *Journal of Turbomachinery* 1992; **114**(3): 528–537.
3. Watterson JK. A pressure-based flow solver for the three-dimensional Navier–Stokes equations on unstructured and adaptive meshes. In *25th AIAA Fluid Dynamics Conference*, Colorado Springs, CO, USA, June, 1994. AIAA 94-2358.
4. de Foy B, Dawes W. Unstructured pressure-correction solver based on a consistent discretization of the Poisson equation. *International Journal for Numerical Methods in Fluids* 2000; **34**: 463–478.
5. Parthasarathy VN, Graichen CM, Hathaway AF. A comparison of tetrahedron quality measures. *Finite Elements in Analysis and Design* 1993; **15**: 255–261.
6. Ilinca A, Camarero R, Trépanier JY, Reggio M. Error estimator and adaptive moving grids for finite volumes schemes. *AIAA Journal* 1995; **33**(11): 2058–2065.
7. Barth TJ, Fredrickson PO. Higher order solution of the Euler equations on unstructured grids using quadratic reconstruction. AIAA 93-0013, 1993.
8. Barth TJ. Recent developments in high order k-exact reconstruction on unstructured meshes. AIAA 93-0668, 1993.
9. Aftosmis M, Gaitonde D, Tavares TS. Behavior of linear reconstruction techniques on unstructured meshes. *AIAA Journal* 1995; **33**(11): 2038–2049.
10. Roe PL. Error estimates for cell-vertex solutions of the compressible Euler equations. Technical Report 87-6, ICASE, January, 1987.
11. Giles MB. Accuracy of node-based solutions on irregular meshes. In *11th International Conference on Numerical Methods in Fluid Dynamics*, Williamsburg, VA, USA, vol. 323 of Lecture Notes in Physics. Springer: New York, 1988; 273–277.
12. Baker TJ. Irregular meshes and the propagation of solution errors. In *15th International Conference on Numerical Methods in Fluid Dynamics*, Monterey, CA, USA, June, vol. 490 of Lecture Notes in Physics. Springer: New York, 1996; 209–218.
13. Lele SK. Compact finite difference schemes with spectral-like resolution. *Journal of Computational Physics* 1992; **103**: 16–42.
14. Tam CKW, Webb JC. Dispersion-relation-preserving finite difference schemes for computational acoustics. *Journal of Computational Physics* 1993; **107**: 262–281.
15. Lockard DP, Brentner KS, Atkins HL. High-accuracy algorithms for computational aeroacoustics. *AIAA Journal* 1995; **33**(2): 246–251.
16. Kim JW, Lee DJ. Optimized compact finite difference schemes with maximum resolution. *AIAA Journal* 1996; **34**(5): 887–893.
17. Tang L, Baeder JD. Uniformly accurate compact difference schemes. In *13th AIAA Computational Fluid Dynamics Conference*, Snowmass Village, CO, USA, 1997. AIAA 97-2093.
18. Lindquist DR, Giles MB. A comparison of numerical schemes on triangular and quadrilateral meshes. In *11th International Conference on Numerical Methods in Fluid Dynamics*, Williamsburg, VA, USA, vol. 323 of Lecture Notes in Physics. Springer: New York, 1988; 369–373.
19. Holmes DG, Connell SD. Solution of the 2D Navier–Stokes equations on unstructured adaptive grids. AIAA 89-1932, 1989.
20. Hirt CW, Cook JL. Calculating three-dimensional flows around structures and over rough terrain. *Journal of Computational Physics* 1972; **10**: 324–340.
21. Zingg DW, Lomax H. Finite difference schemes on regular triangular grids. *Journal of Computational Physics* 1993; **108**: 306–313.
22. Pulliam TH. Artificial dissipation models for the Euler equations. *AIAA Journal* 1986; **24**(12): 1931–1940.
23. Belov A, Martinelli L, Jameson A. A new implicit algorithm with multigrid for unsteady incompressible flow calculations. In *33rd Aerospace Sciences Meeting and Exhibit*, Reno, NV, USA, 1995. AIAA 95-0049.
24. Belov A, Martinelli L, Jameson A. Three-dimensional computations of time dependent incompressible flows with an implicit multigrid-driven algorithm on parallel computers. In *15th International Conference on Numerical Methods in Fluid Dynamics*, Monterey, CA, USA, June, vol. 490 of Lecture Notes in Physics. Springer: New York, 1996; 430–437.
25. Williamson CHK. Defining a universal and continuous Strouhal–Reynolds number relationship for the laminar vortex shedding of a circular cylinder. *Physics of Fluids* 1988; **31**: 2742–2744.

